

Mechanical properties of stabilized zirconia nanocrystalline EB-PVD coating evaluated by micro and nano indentation

Meysam KESHAVARZ^{*}, Mohd Hasbullah IDRIS, Norhayati AHMAD

Department of Materials Science and Engineering, Faculty of Mechanical Engineering, Universiti Teknologi Malaysia, 81310 UTM Johor Bahru, Johor, Malaysia

Received: May 16, 2013; Revised: August 25, 2013; Accepted: August 26, 2013

©The Author(s) 2013. This article is published with open access at Springerlink.com

Abstract: Yttria-stabilized zirconia (YSZ) thin nanocrystalline coatings at different substrate preheating temperatures were deposited via electron beam-physical vapour deposition (EB-PVD). Nanocrystalline ZrO_2 - Y_2O_3 was deposited on the bond coat in order to compensate for the coefficient of thermal expansion (CTE), which can be functionalized as a thermal barrier coating (TBC). The aim of this study was to evaluate mechanical properties with respect to adhesion of zirconia nanocrystalline's top ceramic layer to the interfacial bond coat by utilizing micro and nano indentation tests. In the present paper, the structural studies were carried out using X-ray diffraction (XRD) analysis of coating content (8 mol% of Y_2O_3). The tetragonal phase of stabilized zirconia was observed. Field emission scanning electron microscopy (FESEM) and atomic force microscopy (AFM) were employed to characterize the coatings' morphology and microstructure. The mechanical behavior of ZrO_2 - Y_2O_3 thin films under point loading conditions was studied by nanoindentation using a Berkovich indenter with 130 nm tip radius. Therefore, adhesion of top coat to the interfacial underlying metallic bond coat known as MCrAlY (M = Ni, Co) was estimated according to the highest peak load tests; for a 120 mN peak load, the film manifested tolerable adhesion properties. Moreover, nanoindentation of ZrO_2 - Y_2O_3 nanostructure deposited at 1050 °C substrate preheating temperature produced the highest hardness value of about 21.7 GPa. Vickers micro hardness was utilized with the aid of the Tabor equation in order to achieve deeper insight into the correlation between adhesion and deposition process parameters.

Keywords: zirconia; nanoindentation; nanocrystalline; electron beam-physical vapour deposition (EB-PVD); thermal barrier coating (TBC)

1 Introduction

Zirconia is a technological material applied in a variety

of areas such as optical coatings [1], chemical sensors [2], in addition to hard and protective applications at high temperatures like thermal barrier coatings due to thermal stability of the nanocrystalline coating under long-term service at high temperature [3–7]. Zirconia coating is a reliable material in plenty of wear-resistant applications at elevated temperatures. Thermal barrier

^{*} Corresponding author.
E-mail: kmeysam2@live.utm.my

coating (TBC) systems are indispensable for utilization in gas turbine engines to decrease thermal effect and enhance turbine efficiency by considerably raising applied gas temperatures [4,8]. TBCs are typically composed of an underlying metallic bond coat known as MCrAlY (M=Ni, Co) acting as an oxidation resistant layer, and yttria-stabilized zirconia (YSZ) as a ceramic top coat that provides thermal insulation toward the metallic substrate [7,9]. Due to low thermal conduction, an outer ceramic layer is required. In most cases, ZrO_2 - Y_2O_3 has one of the lowest thermal conductivity values at high temperatures, with a rank of 2.3 W/(m·K) at 1000 °C for 100% density and a thermal expansion rank of $11 \times 10^{-6} (\text{°C})^{-1}$ [10,11]. In this study, YSZ coating was employed on account of hot corrosion protection at high temperatures, as well as thermal strike resistivity to the components. Thus, this system known as TBC is vastly employed in numerous applications such as turbine engine blades and gas turbines [3,12–14]. Inter-metallic alloy based on gamma titanium aluminide was chosen as a substrate. γ -TiAl has the potential to be an important structural material in high-temperature aerospace and automotive applications. The major advantage of γ -TiAl-based super alloy is its low density (3.7–3.9 g/cm³) compared to the conventional nickel-based super alloy which is roughly three times heavier [15–19]. Applying this type of coating involves operations in a broad range of temperatures and thermal expansion, producing high residual stresses and micro cracks leading to delamination and spalling of coatings. The most durable TBCs are widely applied by either air plasma spraying (APS) or electron beam-physical vapour deposition (EB-PVD) [14,20]. EB-PVD endows the advantage of outstanding strain tolerance and thermal shock resistance behavior of the coatings due to their segmented columnar microstructure [4,5,21]. Moreover, it has been reported that low modulus zirconia structures applied by EB-PVD demonstrate higher thermal cyclic life compared with the best plasma-sprayed coatings. In addition, substrate temperature has a profound influence on deposited coating which means the microstructure of YSZ could vary in either a columnar or equiaxed manner as a result of temperature variations of the substrate [5,9,14]. Thus, substrate preheating is typically performed to obtain durable

coating adhesion (i.e., $T/T_m = 0.5$, where T is the substrate temperature and T_m is the melting point of the deposited material). The transition temperature from the columnar structure to the equiaxed structure is at a ratio of deposition temperature to melting temperature of 0.42 [22]. The substrate temperature, target-to-substrate distance and evaporation energy are considered to be the determining parameters for obtaining adhesive coating. The study of mechanical properties has undergone significant development in the last decade. The nanoindentation technique, when combined with finite element studies, demonstrates capabilities of measuring nanocoating hardness and elastic modulus at a few nanometers thickness at both room and high temperatures [23–25]. Moreover, this is an adequate technique for evaluating adhesion and cohesion characteristics; it gives real values without the influence of substrate materials since the maximum indentation depth remains lower than 10%–15% of the coating's thickness [3,26,27]. Furthermore, Vickers micro hardness was utilized together with the Tabor equation in order to determine adhesion as well as durability of the ZrO_2 - Y_2O_3 ceramic top coat over the micro-crack forming in the vicinity of the indentation upon applying a load [26–30]. Nano hardness values obtained with the Nano Indenter XP Machine and a Berkovich indenter reliably correlate with both Rockwell macro hardness and Vickers micro hardness values [31]. In the present paper, field emission scanning electron microscopy (FESEM) investigations on thermally oxidized zirconium oxide nanocrystalline deposited on TBC by EB-PVD were performed in order to get deeper insight into the correlation between adhesion and deposition process parameters.

2 Experiment

2.1 Preparation

The first stage of investigation comprised cutting a 2 mm-thick γ -TiAl plate into square, 10 mm × 10 mm specimens by employing a CNC (computer numerical control) wire cut. The chemical composition of the studied substrate is reported in Table 1.

Table 1 Composition of γ -TiAl substrate

Element	Ti	Al	Nb	Cr
Wight percent (wt%)	48	48	2	2

Prior to deposition, the specimens were abraded with SiC paper of up to 1200 grids, polished by diamond suspension and ultrasonically cleaned in ethanol. Subsequently, the cleaned specimens were immersed in 2% hydrofluoric acid (HF) solution for 1 min, and then washed with distilled water and dried with nitrogen gas in order to achieve a fresh metal surface. The roughness before deposition was measured as tabulated in Table 2.

The pellet-type evaporation target of the bond coat used in the study was made of Ni, Cr, Co, Al and Y elements, whose chemical composition was obtained by energy dispersive X-ray spectroscopy (EDX) analysis (Table 3). EB-PVD single-source coater was used with 1.6 kW beam power and acceleration voltage of 3 kV, while vacuum level was kept at 2×10^{-6} Torr and 750 °C substrate temperature to achieve 3 μm -thick deposition.

The top coat was deposited by a reactive evaporation process. The YSZ was deposited at different substrate preheating temperatures via EB-PVD with 3.5 kW beam power and 5 kV acceleration voltage. Details of deposition conditions are tabulated in Table 4.

Table 2 Surface roughness measurements

Roughness parameter	Roughness value (μm)
R_y (maximum height of the profile)	1.22
R_z (average maximum height of the profile)	0.92
R_a (roughness average)	0.18

Table 3 Composition of bond coat obtained by SEM–EDX analysis

Element	Co	Cr	Al	Y	Ni
Percentage (%)	20–30	18–22	11–13	0.4–0.6	Base

Table 4 Deposition conditions for zirconium films

	Voltage (kV)	Power (kW)	Pressure (Torr)	Substrate temperature (°C)
Bond coat	3	1.6	2×10^{-6}	750
Top coat	5	3.5	1.2×10^{-6}	1050 900 800

2.2 Characterization

All coatings were examined by scanning electron microscopy (SEM), atomic force microscopy (AFM) and EDX to characterize the coatings' microstructure, morphology and chemical composition. Cross-sections of specimens evaluated by SEM indicate an

approximately 3 μm -thick ceramic layer and 3 μm -thick bond coat layer. The coatings' phase composition and preferential crystal orientation were determined with an X'Pert Philips Cu $K\alpha$ X-ray diffractometer. The measurements were made at a 2θ angle ranging from 25° to 100°. Mechanical properties were evaluated by nanoindentation with a Berkovich nanoindenter, which is a triangular pyramid. The nanohardness value is a measure of the pressure required for indentation and not the strength of the material being tested. Despite this, indentation hardness is widely used as a parameter for characterizing the mechanical properties of materials for several reasons. First, indentation hardness tests are relatively easy to perform and provide values with direct measures for loading—bearing capacity of the investigated material. Another reason for the widespread application of hardness tests is closely related to the definition of indentation hardness as a local measure of mechanical properties. For a qualitative evaluation of adhesion, indentations at 120 mN were performed. Low load tests were used to study the effects that deposition parameters had on coating adhesion, hardness and elastic modulus. Furthermore, high peak load tests were done to estimate film adhesion to the interfacial bond coat. Moreover, a Vickers micro indentation test was carried out to determine the adhesion of zircon oxide nanocrystalline top coat at the bond coat's interface. Furthermore, three cross-sectional indentations were taken with the same length from the coating edge to figure out the effect of diffusion on adhesion.

3 Results and discussion

3.1 Coating microstructure

Different substrate preheating temperatures imply variations in coating microstructure. Grain size becomes smaller with decreasing deposition temperature, while coating grains deposited at 800 °C indicate a dense, columnar growth structure as well as very smooth surface that show thin top columns. However, a few small hillocks are observed, owing to either loose atomic mobility during deposition or some surface defects on the substrate responsible for the imperfect growth of some columns, or to the high quantities of material evaporated. Figure 1 exemplifies a typical three-dimensional micrograph of the sample

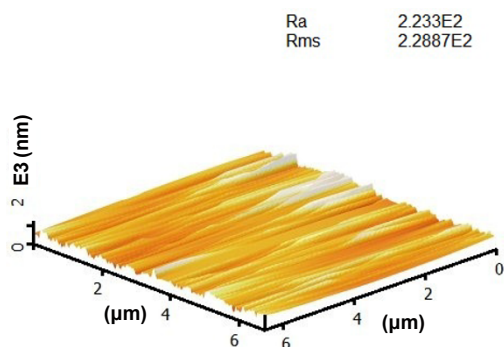


Fig. 1 Three-dimensional AFM of a $\text{ZrO}_2\text{-Y}_2\text{O}_3$ sample surface morphology.

$\text{ZrO}_2\text{-Y}_2\text{O}_3$ (deposited at a partial pressure of 1.2×10^{-6} Torr, 5 kV voltage, 2.5 kW power and 800 °C substrate temperature) obtained by AFM. A decline in surface roughness is observed with increased substrate deposition temperature. As a result, the higher deposition temperature results in thinly sized top columnar growth, and smooth, compact surfaces characterizing lower surface roughness. This effect is due to the elevated atomic mobility that improves the coalescence between grains, and the higher structural densification improved by the bombardment during film growth [11,32].

3.2 Structural characterization

Although ZrO_2 is an interesting material and has many technological applications, it is necessary to impede the tetragonal-to-monoclinic transformation and stabilize high-temperature phases at room temperature for high-temperature applications. This transformation can be suppressed by alloying zirconia with trivalent oxides such as Y_2O_3 , CeO_2 , Gd_2O_3 and Al_2O_3 [15,32]. In order to assess phase composition and other structural information as well as reveal an impression of substrate preheating after depositing the coatings, X-ray diffraction (XRD) was used. Figure 2 presents the XRD patterns for the $\text{ZrO}_2\text{-Y}_2\text{O}_3$ nanostructure coatings. When the substrate temperature goes up from 800 °C to 1050 °C, no significant change in nanocrystalline structure orientation is observed after depositing under stationary conditions. However, column diameter simultaneously expands with

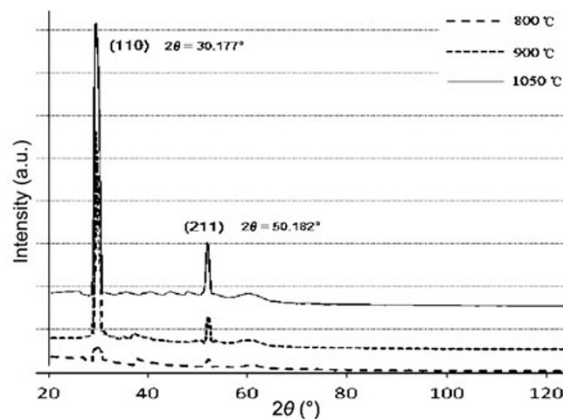


Fig. 2 XRD patterns of the YSZ nanostructure deposited at different preheating substrate temperatures.

increasing temperature, and consequently, the number of columns diminishes. All coatings crystallize in the tetragonal phase. For the coating deposited at 800 °C, no preferential crystalline orientation is observed, and the ratios between the two main diffraction direction intensities, (110) and (211), are approximately equal to 1. In addition, by raising the preheating temperature, a distinctive increase in direction (110) is observed. Only at 1050 °C, a slight indication is given for preferential orientation (211). Preferential orientation is most likely related to the columnar layer structure discerned, especially at higher temperatures (900 °C and 1050 °C). Therefore, final column diameter and general morphological character could be mainly controlled by substrate temperature, rotational speed and surface morphology [4,5].

3.3 Hardness and elastic modulus evaluated by nanoindentation and micro hardness measurements

In this study, hardness and elastic modulus were calculated by Berkovich nanoindentation measurements. The Oliver–Pharr theory was used as a physical principle and model to determine the hardness and elastic modulus from indentation load, or displacement data. A schematic diagram of indentation load (P) versus displacement (h) data obtained during one full cycle of loading and unloading is shown in Fig. 3.

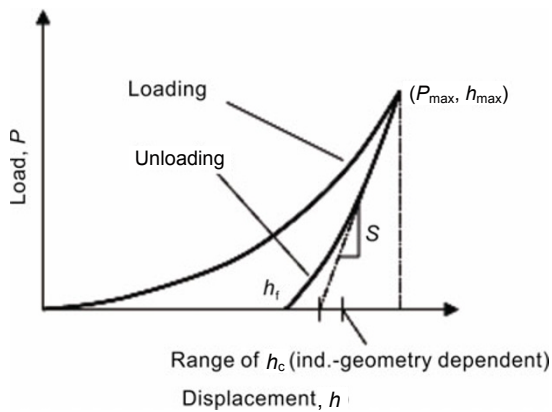


Fig. 3 Schematic illustration of indentation load–displacement data showing important measured parameters during one complete cycle of loading and unloading.

The significant quantities are maximum depth (h_{max}), peak load (P_{max}), final or residual depth after unloading (h_f), and the slope of the upper portion of the unloading curve ($S = dP/dh$). Parameter S is known as elastic contact stiffness. Thus, the hardness and elastic modulus are derived from these quantities. A continuous stiffness measurement technique facilitates monitoring average contact pressure (ACP) for the loading segment. To monitor the ACP in the indent while reloading the indenter, the procedure suggested in Ref. [33] was utilized. Once the contact area is determined, hardness is estimated from

$$H = \frac{P_{max}}{A} \tag{1}$$

where A is the projected contact area at that load, and

$$E_r = \frac{\sqrt{\pi}}{2} \frac{S}{\sqrt{A}} \tag{2}$$

where E_r is the reduced elastic modulus at the deepest point, which can be practically computed from the stiffness, and in turn, contact area can help to generate the contact areas at all depths from the measured stiffness according to

$$A = \frac{\pi}{4} \frac{S^2}{(\beta E_r)^2} \tag{3}$$

where β is a geometrical constant on the order of unity.

The most popular method for justifying contact area was developed by Oliver–Pharr as a theory [33]. The test material’s elastic modulus, E , is calculated from E_r using

$$\frac{1}{E_r} = \frac{1-\nu^2}{E} + \frac{1-\nu_i^2}{E_i} \tag{4}$$

where ν is Poisson ratio for the endurance material, and E_i and ν_i are the elastic modulus and Poisson ratio of the indenter, respectively. For diamond, the elastic constants $E_i=1141$ GPa and $\nu_i=0.07$ are often used [33]. Hardness (H) and elastic modulus (E) values have been plotted in order to assure a non-influential high load peak on the substrate under a 5 mN load. Moreover, rising hardness values as a result of increasing temperatures are noticed. The highest value reaches 21.7 GPa for the sample prepared at a partial pressure of 1.2×10^{-6} Torr, 5 kV voltage, 2.5 kW power and 1050 °C substrate temperature. Similar results are obtained for the elastic modulus. Elastic modulus value is nearly constant for the samples prepared at 1050 °C and 900 °C. A decline in hardness and elastic module values with an increase in peak load is observed for all samples, an effect that could be explained by the contribution of substrate; measurements at higher loads have elevated indentation depths, over 10%–15% of coating thickness. The increase in hardness and residual stress values with elevated temperatures can be explained by a higher densification of nanocoating structure, evident in the sample deposited at 1050 °C. After the deposition process, the cross-sectional hardness of coated specimens shows a significant increase of hardness value at the bond coat’s underlay. According to the Fick’s law, diffusion can take place at high temperatures, thus increasing the occurring hardness due to bond coat and substrate diffusion. A Vickers micro hardness test was done on the cross section close to the bond coat and substrate, as shown in Fig. 4. Each point indicated in Fig. 4 is an average of the hardness value at the same length as the coated edge.

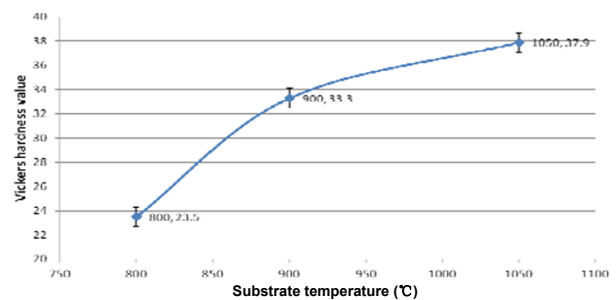


Fig. 4 Vickers micro hardness value on the cross section close to the coated verge of specimens.

A micro indentation test was carried out to qualify the adhesion of zirconia nanocrystalline's top coat to the interface of the underlayer, in this case the bond coat, by applying a square pyramid-shaped Vickers indenter on the surface of the samples deposited at three different preheating temperatures. The micro hardness tests were performed at distinctive constant loads of 5 kg, 10 kg and 20 kg with 10 s holding time, while the indentation results were driven by the Tabor equation. Coating surface delamination in terms of applied load was defined as adhesion strength. The Tabor expression based on the theory of indentation of rigid materials shows that average hardness can be related to the yield stress σ_y .

$$HV = \frac{\text{Indenter force (kg)}}{\text{Surface area of imprint (mm}^2\text{)}} \quad (5)$$

For non-strain hardening materials, the Vickers hardness number defined in the above formula can be related to the constant yield stress, σ_y , by

$$HV = 2.9\sigma_y \quad (6)$$

The Tabor equation defines the relation between load and yield stress σ_y . Figure 5 presents the plotted loads against yield stress σ_y .

Data obtained from Vickers micro hardness is tabulated in Table 5.

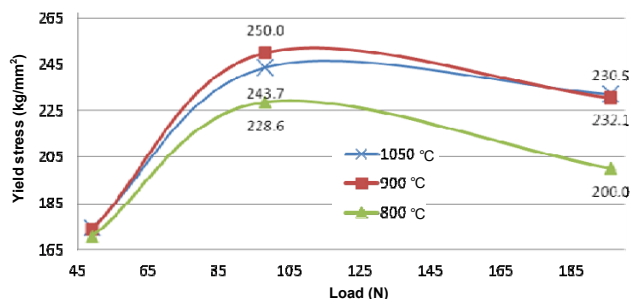


Fig. 5 Load vs. yield stress σ_y .

Table 5 Variation of yield stress by different loads and temperatures

Load (N)	σ_y (MPa)		
	800 °C	900 °C	1050 °C
196.1	1961	2276	2260
98.1	2241	2389	2451
49.0	1674	1703	1745

Different loads were applied by employing micro hardness equipment upon formation of micro cracks in the vicinity of the indentation area. Following indentation, an SEM with a magnification of 100× was

used to evaluate indentation effects. Furthermore, it is revealed that the endurance of components during the indentation test is maximum 20 kg, equal to 784.739 N/m² or Pa to forming crack. The following figures demonstrate the influence of indentation that is applied on the specimen deposited at 1050 °C. By comparison, in Fig. 6, variations in indentation areas versus 5 kg, 10 kg and 20 kg loads at the same magnification can be observed in Figs. 6(a), 6(b) and 6(c), respectively. Moreover, ceramic top coat durability for applied loads up to 20 kg indicates superior adhesion of the ceramic layer to the bond coat deposited at 1050 °C substrate temperature.

A relation between grain size and surface roughness with hardness has been observed, along with the fact that diminishing surface roughness and enlarged grain size cause increasing hardness. This is due to weak

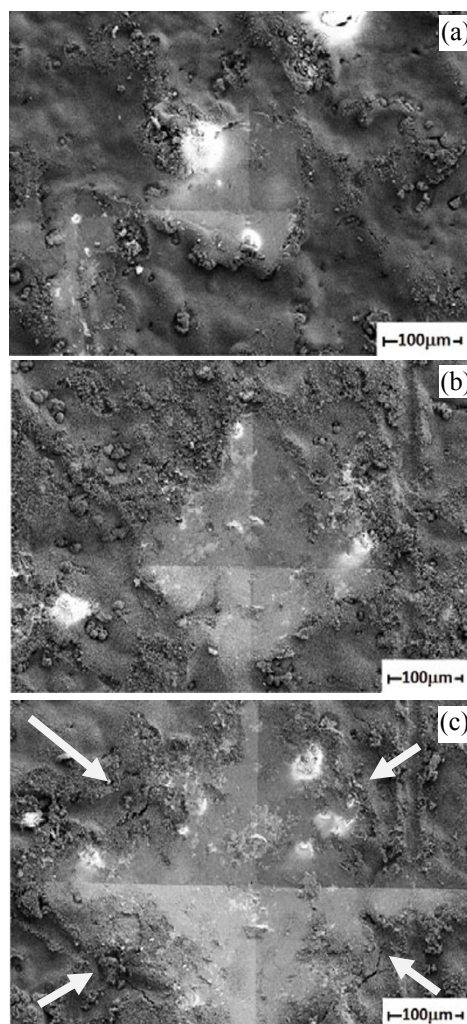


Fig. 6 Indentation effects on the surface of coated samples by applying (a) 5 kg, (b) 10 kg and (c) 20 kg respectively.

boundaries between the small grains, implying a liberty of movement for the indenter. 21.7 GPa, as maximum nanohardness of the sample deposited at 1050 °C, is in accordance with the mentioned relations, because this sample has higher compressive residual stresses, lower grain size and less roughness. Adhesion was evaluated qualitatively by performing nanoindentation measurements at higher loads (120 mN); no coating delamination from the substrate is observed. The material's elastic modulus is also obtained during a nanohardness test. Although the elastic modulus values are beyond the scope of the project, 182 GPa is a relatively constant value with increasing temperature and various indentation loads. It can be inferred that nanohardness testing provides a rational engineering estimation of elastic modulus.

4 Conclusions

With the objective of maintaining the tetragonal phase of zirconia, stabilized nanocrystalline zirconia yttria was deposited by EB-PVD. In order to suppress the tetragonal to monoclinic transformation of deposited zirconia and get the high temperature phases at room temperature, adding 8% Y₂O₃ as a stabilizer to the zirconia matrix facilitated this. All the nanocrystalline zirconia yttria-stabilized coating demonstrated crystalline phases with a predominantly (110) tetragonal direction. Hardness was determined by employing nanoindentation and Vickers micro hardness, and it was observed that by elevating deposition temperatures, values increased. However, elastic modulus remained constant. Deposition hardness reached 21.7 GPa for ZrO₂-Y₂O₃ nanostructured coating deposited at a partial pressure of 1.2×10⁻⁶ Torr, 5 kV voltage, 2.5 kW power and 1050 °C substrate temperature. No film delamination from the underlying bond coat was observed for 120 mN peak load nanoindentation. The compressive residual stresses and coating grain size increased with growing deposition temperature, consequently promoting the hardness values of both nano and micro hardness. Furthermore, in all such depositions, elevated preheating temperatures led to increased grain size and lower surface roughness values. Micro hardness of the deposited specimens was evaluated using a model developed by D. M. Marsh, which is based on the plastic zone analysis below a diamond (Vickers) indenter. From this model, the micro

hardness was observed to increase as the deposition temperature increased, which was almost certainly due to decreasing ceramic material hardness as the defect concentration increased by reducing grain size [22,34]. With higher substrate temperatures during the EB-PVD process, the overall grain size became coarser with a smaller fraction of weak boundaries between the columns, which turned out to be more faceted. This change in microstructure ultimately influenced indentation behavior. Formation phases according to diffusion of the bond coat and substrate caused an increase in cross-sectional hardness as well.

Acknowledgements

The authors would like to acknowledge Ibnu Sina Institute of Fundamental Science Studies and Department of Materials Science and Engineering, Faculty of Mechanical Engineering, Universiti Teknologi Malaysia (UTM) for tests, analysis and supporting this research.

Open Access: This article is distributed under the terms of the Creative Commons Attribution License which permits any use, distribution, and reproduction in any medium, provided the original author(s) and the source are credited.

References

- [1] Gao P, Meng LJ, dos Santos MP, *et al.* Influence of sputtering pressure on the structure and properties of ZrO₂ films prepared by rf reactive sputtering. *Appl Surf Sci* 2001, **173**: 84–90.
- [2] Zosel J, De Blauwe F, Guth U. Chemical sensors for automotive application. *Adv Eng Mater* 2001, **3**: 797–801.
- [3] Andritschky M, Teixeira V, Rebouta L, *et al.* Adherence of combined physically vapour-deposited and plasma-sprayed ceramic coatings. *Surf Coat Technol* 1995, **76–77**: 101–105.
- [4] Schulz U, Saruhan B, Fritscher K, *et al.* Review on advanced EB-PVD ceramic topcoats for TBC applications. *Int J Appl Ceram Tec* 2004, **1**: 302–315.
- [5] Schulz U, Schmücker M. Microstructure of ZrO₂ thermal barrier coatings applied by EB-PVD. *Mat Sci Eng A* 2000, **276**: 1–8.
- [6] Vassen R, Stuke A, Stöver D. Recent developments in the field of thermal barrier coatings. *J Therm Spray Techn* 2009, **18**: 181–186.

- [7] Li M, Sun X, Hu W, *et al.* Thermocyclic behavior of sputtered NiCrAlY/EB-PVD 7 wt.%Y₂O₃-ZrO₂ thermal barrier coatings. *Surf Coat Technol* 2006, **200**: 3770–3774.
- [8] Portinha A, Teixeira V, Carneiro J, *et al.* Characterization of thermal barrier coatings with a gradient in porosity. *Surf Coat Technol* 2005, **195**: 245–251.
- [9] Afrasiabi A, Saremi M, Kobayashi A. A comparative study on hot corrosion resistance of three types of thermal barrier coatings: YSZ, YSZ+Al₂O₃ and YSZ/Al₂O₃. *Mat Sci Eng A* 2008, **478**: 264–269.
- [10] Moskal G. Thermal barrier coatings: Characteristics of microstructure and properties, generation and directions of development of bond. *Journal of Achievements in Materials and Manufacturing Engineering* 2009, **37**: 323–331.
- [11] Singh J, Wolfe DE. Review: Nano and macro-structured component fabrication by electron beam-physical vapor deposition (EB-PVD). *J Mater Sci* 2005, **40**: 1–26.
- [12] Hass DD, Slifka AJ, Wadley HNG. Low thermal conductivity vapor deposited zirconia microstructures. *Acta Mater* 2001, **49**: 973–983.
- [13] DeMasi-Marcin JT, Gupta DK. Protective coatings in the gas turbine engine. *Surf Coat Technol* 1994, **68–69**: 1–9.
- [14] Goward GW. Progress in coatings for gas turbine airfoils. *Surf Coat Technol* 1998, **108–109**: 73–79.
- [15] Copland EH, Gleeson B, Young DJ. Formation of Z-Ti₅₀Al₃₀O₂₀ in the sub-oxide zones of γ -TiAl-based alloys during oxidation at 1000 °C. *Acta Mater* 1999, **47**: 2937–2949.
- [16] Wu Y, Umakoshi Y, Li XW, *et al.* Isothermal oxidation behavior of Ti–50Al alloy with Y additions at 800 and 900 °C. *Oxid Met* 2006, **66**: 321–348.
- [17] Jiang H, Hirohasi M, Lu Y, *et al.* Effect of Nb on the high temperature oxidation of Ti–(0–50 at.%)Al. *Scripta Mater* 2002, **46**: 639–643.
- [18] Kim JP, Jung HG, Kim KY. Al+Y codeposition using EB-PVD method for improvement of high-temperature oxidation resistance of TiAl. *Surf Coat Technol* 1999, **112**: 91–97.
- [19] Schulz U, Terry SG, Levi CG. Microstructure and texture of EB-PVD TBCs grown under different rotation modes. *Mat Sci Eng A* 2003, **360**: 319–329.
- [20] Pakala M, Walls H, Lin RY. Microhardness of sputter-deposited zirconia films on silicon wafers. *J Am Ceram Soc* 1997, **80**: 1477–1484.
- [21] Beake BD, Smith JF. High-temperature nanoindentation testing of fused silica and other materials. *Philos Mag A* 2002, **82**: 2179–2186.
- [22] Courtney TH. *Mechanical Behavior of Materials*. New York: MacGraw-Hill, 1990.
- [23] Mencik J, Quandt E, Munz D. Elastic modulus of TbDyFe films—A comparison of nanoindentation and bending measurements. *Thin Solid Films* 1996, **287**: 208–213.
- [24] Iost A, Najjar D, Hellouin R. Modelling of the Vickers hardness of paint coatings deposited on metallic substrates. *Surf Coat Technol* 2003, **165**: 126–132.
- [25] Lima RS, Kucuk A, Berndt CC. Evaluation of microhardness and elastic modulus of thermally sprayed nanostructured zirconia coatings. *Surf Coat Technol* 2001, **135**: 166–172.
- [26] Limarga AM, Widjaja S, Yip TH. Mechanical properties and oxidation resistance of plasma-sprayed multilayered Al₂O₃/ZrO₂ thermal barrier coatings. *Surf Coat Technol* 2005, **197**: 93–102.
- [27] Portinha A, Teixeira V, Monteiro A, *et al.* Surface analysis of nanocomposite ceramic coatings. *Surf Interface Anal* 2003, **35**: 723–728.
- [28] Tekkaya AE, Lange K. An improved relationship between Vickers hardness and yield stress for cold formed materials and its experimental verification. *CIRP Ann-Manuf Techn* 2000, **49**: 205–208.
- [29] Mencin P, Van Tyne CJ, Levy BS. A method for measuring the hardness of the surface layer on hot forging dies using a nanoindenter. *J Mater Eng Perform* 2009, **18**: 1067–1072.
- [30] Singh J, Wolfe DE. Nanostructured component fabrication by electron beam-physical vapor deposition. *J Mater Eng Perform* 2005, **14**: 448–459.
- [31] Oliver WC, Pharr GM. Measurement of hardness and elastic modulus by instrumented indentation: Advances in understanding and refinements to methodology. *J Mater Res* 2004, **19**: 3–20.
- [32] Wiederhorn SM. Fracture surface energy of glass. *J Am Ceram Soc* 1969, **52**: 99–105.